Intermanifold similarities in partial photoionization cross sections of helium

Tobias Schneider

Max Planck Institute for the Physics of Complex Systems, Nöthnitzer Strasse 38, D-01187 Dresden, Germany

Chien-Nan Liu

Department of Physics, Cardwell Hall, Kansas State University, Manhattan, Kansas 66506

Jan-Michael Rost

Max Plank Institute for the Physics of Complex Systems, Nöthnitzer Strasse 38, D-01187 Dresden, Germany

Using the eigenchannel R-matrix method we calculate partial photoionization cross sections from the ground state of the helium atom for incident photon energies up to the $N=9$ manifold. The wide energy range covered by our calculations permits a thorough investigation of general patterns in the cross sections which were first discussed by Menzel and coworkers [Phys. Rev. A **54**, 2080 (1996)]. The existence of these patterns can easily be understood in terms of propensity rules for autoionization. As the photon energy is increased the regular patterns are locally interrupted by perturber states until they fade out indicating the progressive breakdown of the propensity rules and the underlying approximate quantum numbers. We demonstrate that the destructive influence of isolated perturbers can be compensated with an energy-dependent quantum defect.

PACS number(s): 32.80.Fb, 32.80.Dz

I. INTRODUCTION

Consisting of only three particles, two electrons, and a nucleus, the helium atom nevertheless possesses rich dynamics with complex features. Hence, helium has always been a focus of research and it has incessantly been used as a testing ground of fundamental concepts. In every energy regime the correlated dynamics of the two electrons can be probed by photon impact. This has been the most precise method of investigation in terms of energy resolution although some limitations exist since only those excited states can be accessed whose population is allowed via dipole selection rules from the initial state (usually the ground state). The domain of high double excitation can be scrutinized in greater detail with the advance of the experimental and theoretical tools available. A leading theme in these studies is the exploration of regularities in the observables of this classically chaotic three-body Coulomb system. Moreover, one would like to know how chaotic features emerge when the double-ionization threshold is approached by increasing the energy.

Most experiments have concentrated on total photoabsorption cross sections [1–4]. This is also true for calculations using the method of complex rotation which have reached the highest excitation energy so far. The reason is simply that complex rotation allows for the most effective computation of resonances in terms of their complex energies (where the real part is the energy position and the imaginary part half the resonance width). However, these widths are total widths and only nondifferential observables such as the total photoabsorption cross section can be constructed without losing the effectivity of the approach [5–8].

Yet, as has been demonstrated recently, interesting additional features such as radiative and relativistic effects emerge by, e.g., measuring the photon emission following the photo excitation [9–12]. It turns out that this signal reveals the splitting of the He$^+$ threshold due to spin-orbit coupling. Moreover, in some experiments [13,14] partial photoionization cross sections following photoabsorption into doubly excited states have been measured, most recently up to energies of the $N=5$ excitation threshold of He$^+$ [15]. In the latter work similarities between partial cross sections belonging to different manifolds have been observed and related to the propensity rules for doubly excited states [16–18]. This type of similarity has to be distinguished from *intra*manifold similarities of partial photo cross sections such as mirroring and mimicking, as first noted by Liu and Starace [19].

In the present paper, we explore the origin of *inter*manifold similarities of partial photoionization cross sections in detail. As a function of increasing excitation energy we will describe and explain how these similarities emerge and begin to disappear again for very high excitation. To this end, we have calculated the partial ionization cross sections up to the ninth threshold of He$^+$. The corresponding energies are much higher than those which were reached previously, experimentally as well as numerically. This allows us to work out the similarities of the cross-section pattern across eight manifolds and to illustrate in detail how the propensity rules lead to those similarities. Our results confirm Menzel's conclusions for the energy regime he considered. At higher excitation energies, perturber states seem to destroy the similarity pattern. However, as we will show, a regularization based on an energy-dependent quantum defect can be introduced which restores the similarities even in the presence of isolated perturbers. The paper is organized as follows: In Sec. II, we present the partial cross sections and briefly describe computational details. In Sec. III, we briefly summarize the propensity rules for dipole excitation and for autoionization of two-electron resonances, as well as their classification schemes. We also recall adiabatic two-electron potential curves which facilitate the understanding of the classification and propensity rules, before we formulate the

general scheme of the intermanifold patterns with the help of the propensity rules. In Sec. IV, we interpret the patterns of the partial cross sections across the manifolds with this scheme. The paper ends with a summary in Sec. V.

II. PARTIAL PHOTOIONIZATION CROSS SECTIONS OF HELIUM UP TO $N=9$ LEVEL OF He$^+$

A. Numerical procedure

In the present paper, the eigenchannel R-matrix method [20,21] combined with a close-coupling scheme [22] is employed in order to calculate the partial cross sections for single photoionization of the helium atom.

The eigenchannel R-matrix method has been successfully applied to single photoionization [23] and photodetachment [24] of atomic systems with two active electrons. The most important concept of the R-matrix theory is to partition the configuration space into two regions, namely, the reaction region, where the short-range interactions between one particle and a compact target are complicated, and the external region, where the system can be reduced to a two-body problem involving long-range interactions. For the current paper, the reaction region is that part of six-dimensional configuration space for which both electrons lie within a sphere of radius r_0. The reaction surface Σ is the set of points for which $\max(r_1, r_2) = r_0$, where r_1 and r_2 are the electron distances from the nucleus. The method has been described in detail in the literature [21,22,25]. Therefore, we present here only a brief overview and some numerical details.

Within the reaction region, using a set of Slater determinants composed of properly chosen one-electron orbitals, the electron-electron interaction is fully taken into account by applying bound-state configuration interaction techniques. At a given energy the eigenchannel R-matrix method aims to determine varationally a basis set of wave functions, the so-called R-matrix eigenchannel wave functions, which are orthogonal and complete over the reaction surface Σ enclosing the reaction region, and their negative logarithmic derivatives being constant over Σ. The helium wave functions of experimentally observed channels can be represented by linear combinations of the eigenchannel wave functions thus constructed within the reaction region.

In the external region, since only single ionization processes are considered, it is assumed that there is only a single electron while the other electron is bound. Instead of applying the conventional multichannel quantum defect theory [21], Pan *et al.* [22] developed an approach using a close-coupling scheme to obtain a basis set of multichannel wave functions which describe the outgoing electron and the residual ion. In addition to the Coulomb potential, all multipole interactions in the external region are included numerically to account for the polarization of the residual ion. Note that, although the asymptotic behavior of a one-electron continuum wave function in a Coulomb field is well known [26], this description of a singly ionized state in a two-electron atom is exact only at an infinite distance from the nucleus. Since one can only integrate the close-coupling equation starting from a finite distance, we use WKB representations [27] for the wave function instead at a suitably large dis-
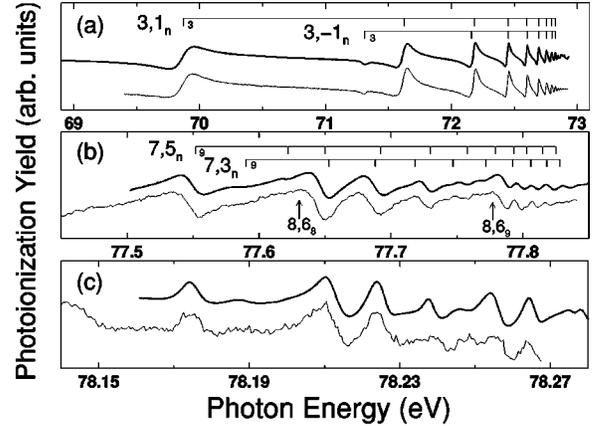

FIG. 1. Calculated total photoionization cross section in comparison with experimental results of Refs. [4,29] below the thresholds (a) $N=3$, (b) $N=7$, and (c) $N=9$. The theoretical data (thick lines) have been shifted upwards to allow for an easier comparison with the experiment (thin lines). Moreover, the numerical data have been convoluted with a Gaussian of 5 meV width for $N=3$, 7, and 2 meV for $N=9$. In (a) and (b) the positions of the resonance states of the two strongest Rydberg series are indicated [6]; for an explanation of the quantum numbers, see Sec. III.

tance. To describe an experimentally observed channel, one has to form a linear combination of these multichannel basis wave functions according to the incoming-wave boundary condition [22].

By matching the linear combinations of the multichannel basis functions for the two regions, one can determine the exact final state wave-functions $\Psi_i^{(-)}$ which describe the experimentally observed channels i. The partial cross sections can be calculated according to the standard formula [28]:

$$\sigma_i = \frac{4\pi^2 \omega}{c} |\langle \Psi_i^{(-)} | D | \Psi_0 \rangle|^2, \tag{2.1}$$

where ω is the photon energy, D is the dipole operator, and c is the speed of light. The wave-function Ψ_0 in Eq. (2.1) denotes the helium ground state.

In the present paper, the radius r_0 of the R-matrix sphere is chosen to be 200 a.u. A total of 1080 closed-type (i.e., zero at the radius r_0) and 20 open-type (i.e., nonzero at the radius r_0) one-electron wave functions with orbital angular momentum up to nine are included. 9610 closed-type two-electron configurations are included in the calculation for the final state wave function. For each channel in which one electron can escape from the reaction region, two open-type orbitals for the outer electron are included in addition to the closed-type basis set. For a given photon energy, besides all open channels, relevant closed channels are also included in the calculations (cf. [22]).

B. Typical cross sections

Our calculated total photo cross section below the $N=3,7$, and 9 threshold are shown in Fig. 1 together with experimental data by Kaindl and his group [4,29]. Since no
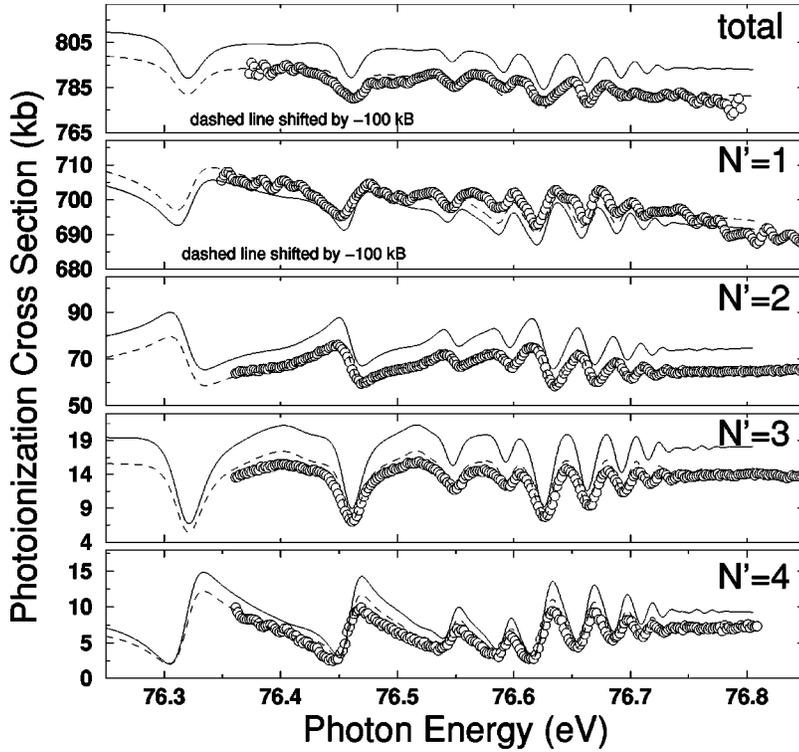
FIG. 2. Calculated (absolute) total and partial cross sections are compared to experimental data (circles) of Menzel *et al.* [15] in the region of the $N=5$ resonances. Calculation in velocity gauge, solid lines; calculation in acceleration gauge, dashed lines; experiment, open circles. The numerical results have been convoluted with a Gaussian of 5 meV width. The acceleration gauge result for $N'=1$ (and consequently for the total cross section) is shifted by -100 kb.

absolute photoionization yields are measured in these experiments we have scaled the experimental data to our results. As can be clearly seen the calculated cross section is in excellent agreement with the experimental one.

Figure 2 shows the total and partial cross sections below the $N=5$ threshold of He^+. Note that below a given threshold N we are dealing with $N-1$ partial cross sections $\sigma_{N,N'}$ ($N'=1,\ldots,N-1$), where $N'(<N)$ denotes the principal quantum number of the residual helium ion. Hence, in the case of the $N=5$ threshold we are concerned with four partial cross sections, namely, $\sigma_{5,1}\ldots\sigma_{5,4}$. The agreement with existing experimental data [15] on an absolute scale is, in general, good. Interestingly, the cross section in acceleration gauge (dashed) is higher than in velocity gauge (solid) and higher than the experiment for the partial cross section $N'=1$. For all other partial cross sections the velocity gauge result is too high and the acceleration gauge matches the experiment better. The total cross section behaves as the $N'=1$ partial cross section by which it is dominated. This observation of numerical accuracy points to a fundamental difference of the $N'=1$ cross section compared to all other partial cross sections which is also confirmed by the fact that $N'=1$ takes about 90% of the yield while the yield for the higher partial cross sections decreases with increasing N' but only slightly.

Since we focus on the general patterns of the partial cross sections which agree in both gauges very well with experiment the minor discrepancies in the absolute value are of no concern.

1. Partial cross sections of resonances converging to the $N=9$ threshold of He^+

The ninth threshold is only about 0.67 eV below the double ionization threshold. Partial cross sections for the N

$=9$ manifold have neither been measured nor been calculated so far. Based on the good agreement of the total cross section with the experiment (see Fig. 1) we believe that our calculation in this energy range is still reliable. As can be seen in Fig. 3 the regular sequences of Rydberg series observed for lower manifolds appear to be lost. However, even if a regular Rydberg progression exists it is very difficult to identify it at a finite energy resolution since the peaks accumulate towards threshold. For this reason we will use an alternative way to represent the cross section data.

2. Unfolding cross sections

To make all peaks of a Rydberg progression in a cross section clearly visible which is particularly important for analyzing similarities in the patterns of cross sections we re-parametrize the energy according to the effective quantum number [30]. An ideal unperturbed Rydberg series converging to a threshold N of the He^+ ion would have equidistant peaks as a function of the effective quantum number

$$\nu_N(E)=\sqrt{\frac{\mathcal{R}}{I_N-E}},\qquad(2.2)$$

where $\mathcal{R}$ is the Rydberg constant, and $I_N=4\mathcal{R}/N^2$ denotes the Nth ionization potential ($I_\infty=0$ a.u.) of He^+. In Fig. 4 we show partial cross sections below the $N=4$ threshold where we have scaled the energy axis according to Eq. (2.2). The constant spacing of the resonances indicates unperturbed Rydberg series. Note also that the two partial cross sections $He^+(N'=1)$ and $He^+(N'=3)$ in Fig. 4 behave quite similarly while $He^+(N'=2)$ mirrors their pattern. This mirroring and mimicking behavior of partial photo cross section is a universal *intra*manifold feature [19].
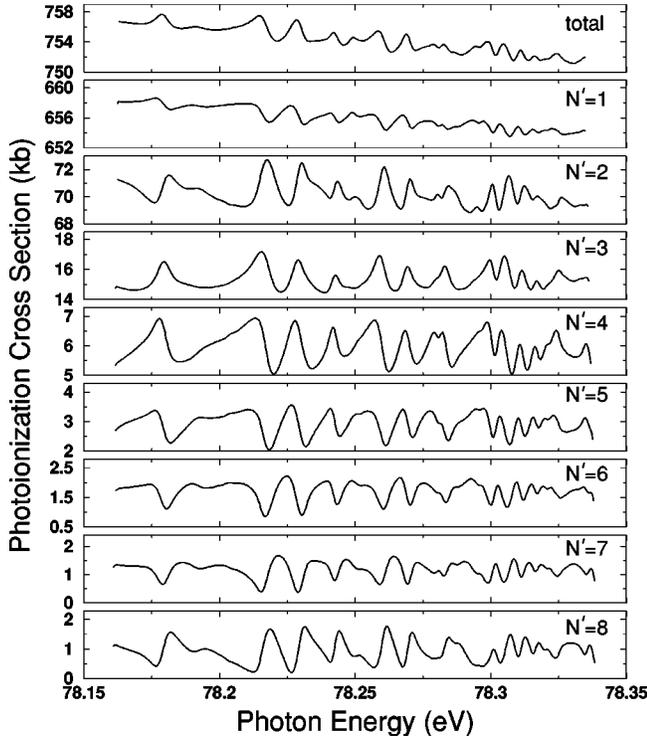
FIG. 3. Calculated partial photoionization cross sections below the $N=9$ threshold (using velocity gauge). The data are convoluted with a Gaussian of 1 meV width.

So far, we have presented illustrative examples for the cross sections to highlight the accuracy of our calculation. We will systematically present the *inter*manifold similarities between certain partial cross sections and discuss their origin in the next two sections. The relations between certain chains of partial cross sections as well as the interpretation which resonances contribute to them is based on the existence of
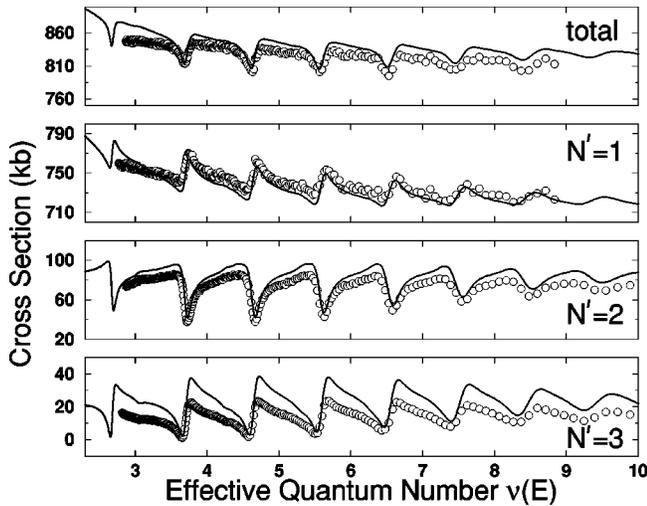

FIG. 4. Partial cross sections as a function of the effective quantum number $\nu_4(E)$ below the $N=4$ threshold. Due to an energy-independent quantum defect the resonance spacings are equal. Theory (velocity gauge), solid lines; experiment [15], open circles. The numerical data are convoluted with a Gaussian of width 5 meV.
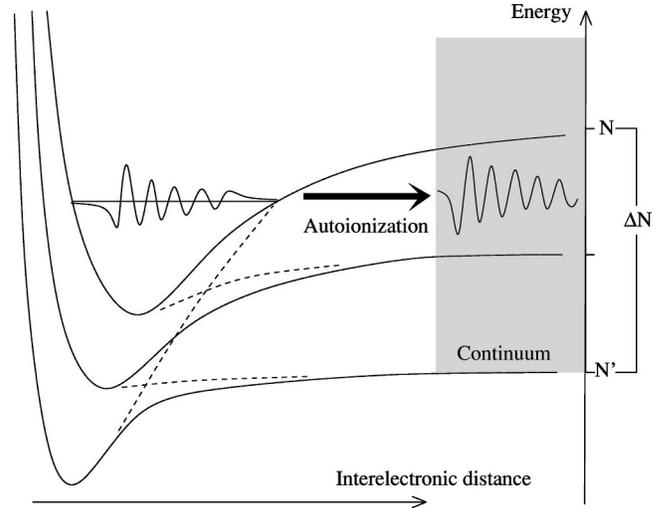

FIG. 5. Schematic representation of adiabatic potential curves. In the adiabatic picture the resonances appear as vibrational eigenstates. The mechanism of autoionization relies on nonadiabatic transitions in this description. The dashed lines indicate the avoided crossings of the potential curves which play an important role in the derivation of the propensity rules (see Ref. [6]).

approximate quantum numbers and propensity rules for the resonances which we will discuss first.

III. APPROXIMATE QUANTUM NUMBERS AND PROPENSITY RULES

Over the last 20 years a scheme of approximate quantum numbers for doubly excited states has been developed which reflects the correlated two-electron dynamics. They have been expressed as $_N(K,T)^A$ by Herrick and coworkers [31] and assigned to hyperspherical potential curves by Lin [32]. Feagin and Briggs [33] gave a justification for the quantum numbers in terms of constants of motion for a separable Hamiltonian which arose from the introduction of the so-called molecular adiabatic approximation. This approximation is similar to the Born-Oppenheimer approximation for a diatomic molecule, namely, H_2^+, but with reversed roles of electrons and nuclei. In two-electron atoms it is the interelectronic axis R which is taken as adiabatic, i.e., slow variable in analogy to the internuclear axis in H_2^+. In this picture the doubly excited states naturally appear as vibrational eigenstates in the adiabatic potential curves (cf. Fig. 5).

Probably the most simple way of understanding the quantum numbers is to interpret them as the Stark quantum numbers of the inner electron whose Coulomb motion is perturbed by the electric field of the outer electron. The quantum numbers remain the same along a Rydberg series when the outer electron's quantum number n increases to infinity (single ionization limit) and the inner electron remains in the Nth excited state of the ion, where $N=N_1+N_2+m+1$ is the sum of the Stark quantum numbers. Note, that the classification will be relevant to understand the pattern in partial ionization cross sections since it is also applicable to singly ionized two electron states (i.e., continuum states). The Stark quantum numbers (often called

parabolic quantum numbers) are related to Herrick's scheme by $T = m$ and $K = N_2 - N_1$. The label A denotes the symmetry with respect to the line $r_1 = r_2$ in the wave function where the r_i are the electron-nucleus distances. The complete signature of a two-electron resonance is then $[N_1 N_2 m]_n^A$ or $_N(K,T)_n^A$. For the classification of resonance states in helium photoionization from the ground state one very often uses a simplified Herrick's notation, namely, N,K_n, where the other quantum numbers are redundant due to the dipole selection rules (see Fig. 1). For a more complete comparison between the different quantum numbers see [6,18].

The approximate constants of motion for correlated two-electron dynamics expressed through the approximate quantum numbers imply a nodal structure for the respective resonance states [34]. In turn, this nodal structure leads to preferences for autoionization [16] and (radiative) dipole transitions [35].

A. Propensity rules for radiative transitions

Propensity rules for radiative transitions can be derived by analyzing the dipole matrix elements according to the nodal structure of the resonance wave functions, which is a simple analytical task on the potential saddle for $2\vec{r} \equiv \vec{r}_1 + \vec{r}_2 = 0$. This region in configuration space is most relevant for symmetrically excited electrons with $N \approx n$. It corresponds to the equilibrium geometry of a linear ABA molecule [36]. Not surprisingly, the relevant quantum number

$$v_2 = 2N_1 + m \qquad (3.1)$$

for radiative propensities quantizes the twofold degenerate bending motion of triatomic molecules and can be derived by normal mode analysis about the saddle point [35,37]. Dipole matrix elements within the saddle approximation follow the selection rule

$$\Delta v_2 = 0, \pm 1 \qquad (3.2)$$

that survives for the full dynamics as a propensity rule. Here, we are interested in photoabsorption into doubly excited states from the ground state of helium. The final $A = +1$ states with the admixture of lower channels for the relatively best overlap with the ground state can only be $m = +1$ states due to the $^1P^o$ symmetry. Therefore, we expect a preference for

$$\Delta v_2 = 1 \qquad (3.3)$$

transitions (i.e., $\Delta m = 1$). In each manifold N there is only one series $[0(N-2)1]^+$ fulfilling this condition. This series is commonly referred to as the *principal series* in the literature. Other series (with $A = +1$) are also populated without the preference of $\Delta N_1 = 0$. However, they carry much less oscillator strength.

B. Propensity rules for nonradiative transitions

The mechanism of autoionization relies on nonadiabatic transitions in the (molecular) adiabatic picture. The rules for

autoionization can be stated by establishing a preference for nodal changes in the wave function.

Most easily, N_2 can be changed which is the preferred decay mode. This is achieved in the molecular description (as well as in the hyperspherical one) by so-called radial coupling matrix elements which are large between states which differ only in N_2. Rotational coupling is only slightly less effective and changes the quantum number m. Finally, there is no mechanism to change N_1. Hence, a resonance decays only through changing N_1 if no other possibility exists.

In parallel, the symmetry A plays an important role. In general, states with $A = +1$ decay more easily than states with $A = -1$ which can be seen from the narrower avoided crossings for $A = +1$ leading to larger radial couplings compared to $A = -1$ states. We may summarize the propensity rules for autoionization [16] according to the relative efficiency of the underlying decay mechanism:

$$(A) \quad \text{reduction of } N_2, \qquad (3.4a)$$

$$(B) \quad \text{change of } m, \qquad (3.4b)$$

$$(C) \quad \text{reduction of } N_1. \qquad (3.4c)$$

These propensity rules group the $^1P^o$ resonant states of helium into three classes I–III with typical widths separated by at least two orders of magnitude, $\Gamma_I : \Gamma_{II} : \Gamma_{III} \approx 10^4 : 10^2 : 1$. Since the propensities depend on the nodal structure $[N_1 N_2 m]$ of the inner electron, they hold for entire Rydberg series (different n) characterized by a single $[N_1 N_2 m]$ configuration. States of class III for $^1P^o$ resonances are restricted to the $[(N-1)00]^-$ configurations, which enforce decay through a $\Delta N_1 \neq 0$ transition (C).

C. Propensities for partial photoionization cross sections

We proceed now to formulate the conditions for the similarity in patterns of partial photo cross sections based on the existing propensity rules. The propensity rule (A) characterizes by far the most important mechanism for autoionization and it is this decay mechanism which also determines the similarity patterns.

1. Configurations, manifolds, and chains

So far we have already used the terms configuration and manifold. A *configuration* is a set of two-electron states characterized by the quantum numbers $[N_1 N_2 m]^A$ which refer to the state of the inner electron in the correlated two-electron state. A *manifold* N of two-electron states contains all configurations whose quantum numbers add up to $N = N_1 + N_2 + m + 1$. Physically, one can think of N being the principal quantum number of the electron in the He^+ ion which would remain if the outer electron would be taken away. In the adiabatic picture a configuration is represented by a potential curve (see Fig. 5). This illustrates that the actual state of the outer electron is not specified for a configuration. It can be a bound state with quantum number n in the potential curve corresponding to a resonance for the two-electron system.

These types of states we call in the present context *intermediate configuration*. The outer electron can also be in the continuum characterized by the potential of the configuration of the inner electron. These types of states we call *final configuration*. It is important to realize that all the propensity rules refer to the nodal character induced by the configurations only, i.e., to a first approximation, the state of the second electron being a Rydberg electron n or in the continuum is irrelevant for these propensities. However, this does not mean that we deal with independent electron states. Rather the Stark quantum numbers of a configuration for the inner electron characterize a whole set of correlated two-electron states.

Photoionization proceeds from the initial state (here the ground state of helium) either directly or via a resonance of the intermediate configuration to the final configuration. Particularly the partial cross sections $\sigma_{N,1}$ have a strong direct channel (simply the photoionization of one of the electron). This is seen in the large smooth background cross section (e.g., Fig. 2) for the $N'=1$ partial cross sections.

To form a partial cross section $\sigma_{N,N'}$ one has to take into account all accessible intermediate and final configurations. The propensity rules can be used to structure the contributions of different configurations and they determine which of these configurations contribute dominantly to the cross section.

2. Chain of similar partial cross sections with dominant configurations only

Suppose we excite from the ground state only the configurations $[0(N-2)1]^+$, $N=2,3,\ldots$, i.e., all the principal series. This yields partial cross sections $\tilde{\sigma}_{N,N'}$ which already show the main features of the physical cross sections, and consequently, their similarity patterns. The most efficient autoionization mechanism is governed by propensity rule (A), i.e., by reducing the quantum number N_2. Hence, the dipole excited intermediate configuration $[0(N-2)1]^+$ will lead to a dominant final configuration $[0(N'-2)1]^+$ for the partial cross section $\tilde{\sigma}_{N,N'}$ with the change in N_2 being $\Delta N = N-N'$. The idea is now that partial cross sections in different manifolds look similar if their final configurations have an identical difference $\Delta N = N-N'$ in the quantum number N_2 with respect to the respective intermediate configurations. Figure 6 shows the partial cross sections across the manifolds N with $\Delta N=1$. Apart from the first cross section $\sigma_{2,1}$ all patterns look fairly similar as predicted. There are local perturbations marked as "PT" and one also notes that the similarities become weaker for the highest cross section shown, namely, $\sigma_{9,8}$. Both of these anomalies we will discuss later, after we have explained why $\sigma_{2,1}$ looks so different. This is easy to understand because the principal intermediate configuration $[001]^+$ in the $N=2$ manifold cannot decay through ΔN_2 to the $N=1$ manifold since $N_2=0$ to begin with. Rather, $[001]^+$ decays by changing A and m to $[000]^-$ which is not the preferred decay route.

Therefore, a chain of similar cross sections has a lower end defined by the (N_1,m) quantum numbers of the contrib-
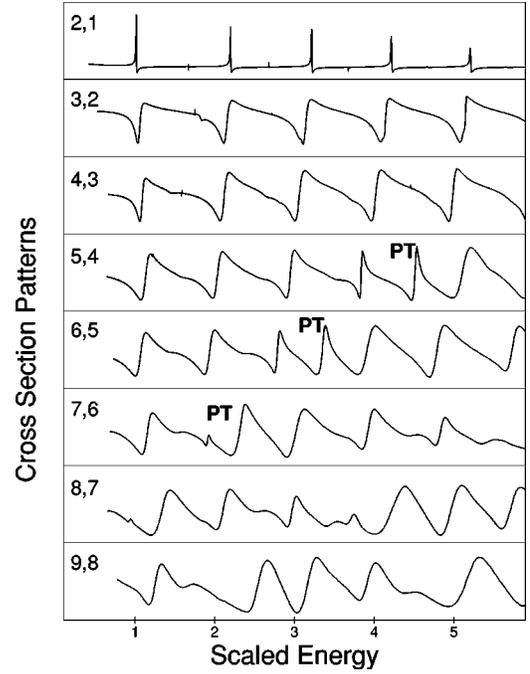
FIG. 6. Partial cross sections with $\Delta N = N-N' = 1$. The energy axis of each panel is scaled according to Eq. (2.2). Additionally, each of the individual cross sections is horizontally shifted by a constant quantum defect in order to approximately align the resonances of the principal series. The numbers on the left stand for N,N'. The cross section $\sigma_{N,N'}$ with $N\geq 6$ are convoluted with a Gaussian of width 1 meV. A few perturbers are indicated by "PT."

uting chain of configurations and its difference $\Delta N_2 = N - N'$ in N_2:

$$N_{\min} = N_1 + m + \Delta N_2 + 1. \tag{3.5}$$

In our example with $N_1=0$ and $m=\Delta N_2=1$ we have $N_{\min}=3$, therefore, $\sigma_{2,1}$ does not belong to the chain.

3. Partial cross-section chain including all configurations populated

A closer look on Fig. 6 reveals that there is still a small change in the characteristic pattern from $\sigma_{3,2}$ to $\sigma_{5,4}$. The reason is that in addition to the dominant intermediate configuration $[0(N-2)1]^+$ other configurations are populated as well, each of them having its own chain of similar patterns across the manifolds. The actual experimental pattern is the sum of all these patterns. However, each chain has its individual lower end according to Eq. (3.5). For instance the chain fed by the intermediate configuration $[1(N-3)1]^+$ starts in the manifold $N_{\min}=4$ and does not contribute to $\sigma_{3,2}$. In fact excited from the ground state in helium $[0(N-2)1]^+$ and $[1(N-3)1]^+$ are the two strongest intermediate configurations and we expect their chains to be sufficient to understand the evolution of the regularity of the patterns in the partial cross sections which will be discussed in the next section. For simplicity we introduce a short notation

$$\mathcal{C}_{N_1,m}^A(\Delta N_2) \tag{3.6}$$
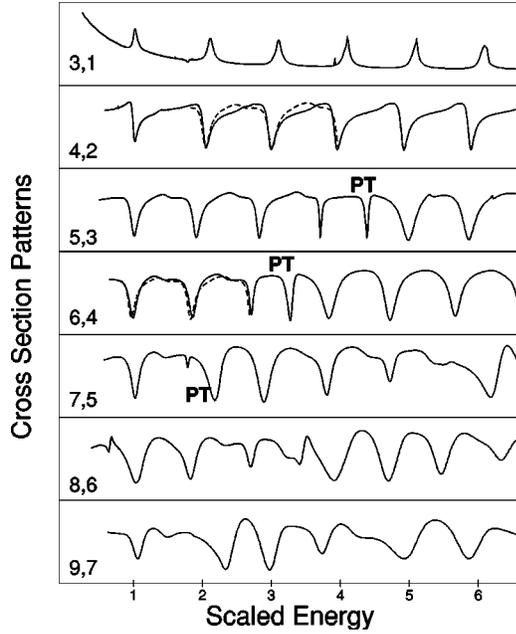
FIG. 7. Same as Fig. 6 but for the $\Delta N=2$ partial cross sections. For comparison a clipping of $\sigma_{N=5,N'=3}$ (dashed line) is shown in the 4,2 and 6,4 panel.

FIG. 8. Same as Fig. 6 but for the $\Delta N=3$ partial cross sections.

to describe the chains where N_1,m,A characterize the intermediate configuration and determine the lower end of the chain $N_{\min}$ according to Eq. (3.5) while ΔN_2 characterizes the type of similar cross sections with $\Delta N=\Delta N_2$ emerging from the chains. So far we have focused on $\Delta N_2=1$ (shown in Fig. 6) with the two dominant chains $\mathcal{C}_{0,1}^+(1)$ and $\mathcal{C}_{1,1}^+(1)$.

IV. SYSTEMATICS IN PARTIAL CROSS SECTIONS ACROSS MANIFOLDS FROM $N=2$ TO $N=9$

We will now test the systematics for the patterns described and illustrated in the last section for $\Delta N_2=1$ with cross sections of $\Delta N_2>1$. Thereby, we will also discuss the phenomenon of perturbers and the slow disappearance of the patterns for very high partial cross sections, as mentioned in the last section.

A. Partial cross sections with $\Delta N=2$

We first discuss the $\Delta N=2$ partial cross sections shown in Fig. 7. The general pattern looks quite different compared to $\Delta N=1$ shown in Fig. 6. However, among each other, the partial cross sections behave similarly as in Fig. 6: The lowest curve $\sigma_{3,1}$ does not match at all the other curves, the next one, $\sigma_{4,2}$, is still slightly different from the higher ones which are quite similar. For $\sigma_{8,6}$ and higher the patterns begin to fade out. We first note that the lowest possible partial cross section for $\Delta N=2$ is $\sigma_{3,1}$. As for $\sigma_{2,1}$ in Fig. 6 the dominant intermediate configuration $[011]^+$ cannot decay according to the preferred propensity rule $\Delta N_2=2$ but must decrease the quantum number m and therefore change the quantum number A from $+1$ to -1 in addition. Hence, $\sigma_{3,1}$ does not belong to the chain of similar cross sections. To the next higher one, $\sigma_{4,2}$ contributes only the chain built on the

principal intermediate configuration $[021]^+$ with $N_{\min}=4$. For $\sigma_{5,3}$ both dominant chains $\mathcal{C}_{0,1}^+(2)$ and $\mathcal{C}_{1,1}^+(2)$ can contribute. Consequently, $\sigma_{5,3}$ is the partial cross section with the lowest N exhibiting the fully developed pattern of $\Delta N=2$ which one sees comparing the clipping of $\sigma_{5,3}$ to $\sigma_{4,2}$ and $\sigma_{6,4}$ (see dashed lines in Fig. 7).

B. Partial cross sections with $\Delta N=3$

These cross sections, shown in Fig. 8, have a characteristic pattern, which is different from the respective groups characterized by $\Delta N=1$ and $\Delta N=2$. Yet, the systematics within the group is again the same as for the other two groups and can be translated by simply increasing N by one: The first cross section $\sigma_{4,1}$ looks extremely different since it does not belong to a chain. To the next one only the chain from the principal intermediate configuration contributes, $\sigma_{6,3}$ contains for the first time the characteristic pattern for $\Delta N=3$. However, since we are already close to $N=8$ where the patterns start to fade out due to a beginning break down of the propensity rules to which we ascribe their existence, we see only two relatively similar cross sections, $\sigma_{6,3}$ and $\sigma_{7,4}$.

We summarize the systematics of the chains in Fig. 9 where all intermediate configurations are shown which can decay according to propensity rule (A) [Eq. (3.4a)]. From Fig. 9 the lower end characterized by N,N' of any chain can easily be determined. For example, $\mathcal{C}_{0,0}^-(\Delta N)$ evokes a pattern with intermediate configurations $[0N0]^-$ already starting at $N'=1$ with $\sigma_{N,N'=1}$ cross sections. However, as repeatedly pointed out, they are too weak to be seen in the cross sections.

1. Role of isolated perturbers

Before the pattern actually breaks down (see, e.g., Fig. 8) it can already be locally distorted by so called perturber states. As is well known from quantum defect theory [38], a

FIG. 9. Compilation of all two-electron configurations (labeled by parabolic quantum numbers), which can decay according to propensity rule (A) [Eq. (3.4a)]. The $+$ and the $-$ signs stand for $A = \pm 1$ and the principal configurations are underlined.

perturber acts in a twofold way on the resonance states to which it couples. First, it shifts their positions ("bunching effect") which is expressed by a jump in the quantum defect. Second, it modulates their linewidth in a Fano-profile-like way. Both effects locally perturb the cross section pattern.

The bunching of the resonances is visible in the cross-sections $\sigma_{N=5,N'}$ and $\sigma_{N=6,N'}$ with the perturbers $N,K_n = 6,4_6$, and $7,5_7$, respectively. The distorting influence on the pattern can be compensated by incorporating the quantum defect $\delta_{N,K_n}(E)$ of the perturbed series. Plotting the cross section against the effective quantum number $\nu_6(E) + \delta_{6,4_n}(E)$, restores the characteristic pattern of the cross section as can be seen in Fig. 10(b). The effective quantum defect compensates the bunching of resonances on the energy axis. Therefore, this kind of disentanglement works well, as long as the effect of the perturber on the width of the resonances is small as it is the case for the cross-sections $\sigma_{N=5,N'}$ and $\sigma_{N=6,N'}$. The perturber $8,6_8$, however, causes a drastic narrowing of the width of the state $7,5_{10}$. This perturbation of the pattern cannot be compensated by expressing the energy in terms of the effective quantum defect. However, the perturbation remains small and local leaving the general pattern still identifiable as one can see in the cross-sections $\sigma_{7,N'}$ of Figs. 6, 7, and 8.

2. Fading out of patterns

Going to higher manifolds the patterns start to fade out. This is certainly due to an increasing number of perturbers. However, in more general terms, this observation indicates the beginning breakdown of approximate quantum numbers and consequently of the propensity rules which govern the patterns. This refers to a situation discussed here with the

FIG. 10. Partial cross section of the $N'=4$ satellite below the $N=6$ threshold (a) as a function of the effective quantum number $\nu_6(E)$ [Eq. (2.2)] and (b) as a function of $\nu_6(E) + \delta_{6,4_n}(E)$, where $\delta_{6,4_n}(E)$ denotes the quantum defect of the series $6,4_n \equiv [041]_n^+$. In (a) the position and the linewidth of the perturber $N,K_n = 7,5_7$ are indicated [6]. In (b) the bunching of the resonances due to the perturber is disentangled restoring the similarity pattern.

principal quantum number n of the outer electron only moderately larger than the principal quantum number N of the inner electron. Clearly, for $n \gg N$ the regime of a (regular) effective one-electron Rydberg series is always approached.

V. CONCLUSIONS

We have presented numerical total and partial cross sections for single photoionization from the helium ground state up to the $N=9$ threshold of He^+. Our calculations were done by using the eigenchannel R-matrix method. We found very good agreement with available experimental data for both the total cross section up to the $N=9$ manifold and the partial cross sections up to the $N=5$ manifold.

A comparison of the partial cross sections $\sigma_{N,N'}$ (N' denoting the state of the residual helium ion) across the manifolds reveals common patterns in the cross sections with the same $\Delta N = N - N'$. The patterns of the principal series dominate with a seizable contribution from strongest secondary series due to the large oscillator strength of these series. The manifestation of the patterns can be attributed to chains of configurations which connect the intermediate configurations of resonance states seen in the cross sections to final configurations in the different continua according to the dominant propensity rule for autoionization.

Starting with the $N=5$ manifold perturbers emerge which locally destroy the general patterns. However, in cases where the perturber mainly leads to a bunching of resonances on the energy axis, a regularization based on energy-dependent quantum defects has been shown to disentangle the spectra and restore the similarity of the patterns. Going to manifolds $N=8$ and higher the patterns start to fade out which finally indicates the breakdown of the propensity rules. This in turn signals the approaching limits of the adiabatic picture and the approximate quantum numbers derived from it.

[1] R. P. Madden and K. Codling, Phys. Rev. Lett. **10**, 516 (1963).

[2] H. D. Morgan and D. L. Ederer, Phys. Rev. A **29**, 1901 (1984).

[3] H. Kossmann, B. Krässig, and V. Schmidt, J. Phys. B **21**, 1489 (1988).

[4] M. Domke, C. Xue, A. Puschmann, T. Mandel, E. Hudson, D. A. Shirley, G. Kaindl, C. H. Greene, H. R. Sadeghpour, and H. Petersen, Phys. Rev. Lett. **66**, 1306 (1991); M. Domke, G. Remmers, and G. Kaindl, *ibid.* **69**, 1171 (1992); M. Domke, K. Schulz, G. Remmers, A. Gutiérrez, G. Kaindl, and D. Wintgen, Phys. Rev. A **51**, R4309 (1995); M. Domke, K. Schulz, G. Remmers, G. Kaindl, and D. Wintgen, *ibid.* **53**, 1424 (1996); K. Schulz, G. Kaindl, M. Domke, J. D. Bozek, P. A. Heimann, A. S. Schlachter, and J. M. Rost, Phys. Rev. Lett. **77**, 3086 (1996).

[5] D. Wintgen and D. Delande, J. Phys. B **26**, L399 (1993).

[6] J. M. Rost, K. Schulz, M. Domke, and G. Kaindl, J. Phys. B **30**, 4663 (1997).

[7] B. Grémaud and D. Delande, J. Phys. B **31**, 1671 (1998).

[8] A. Bürgers, D. Wintgen, and J. M. Rost, J. Phys. B **28**, 3163 (1995).

[9] J.-E. Rubensson, C. Såthe, S. Cramm, B. Kessler, S. Stranges, R. Richter, M. Alagia, and M. Coreno, Phys. Rev. Lett. **83**, 947 (1999); T. W. Gorczyca, J.-E. Rubensson, C. Såthe, M. Ström, M. Agåker, D. Ding, S. Stranges, R. Richter, and M. Alagia, *ibid.* **85**, 1202 (2000).

[10] M K. Odling-Smee, E. Sokell, P. Hammond, and M. A. Mac-Donald, Phys. Rev. Lett. **84**, 2598 (2000).

[11] F. Penent, P. Lablanquie, R. I. Hall, M. Žitnik, K. Bučar, S. Stranges, R. Richter, M. Alagia, P. Hammond, and J. G. Lambourne, Phys. Rev. Lett. **86**, 2758 (2001).

[12] C.-N. Liu, M.-K. Chen, and C. D. Lin, Phys. Rev. A **64**, 010501(R) (2001).

[13] P. R. Woodruff and J. A. R. Samson, Phys. Rev. A **25**, 848 (1982).

[14] M. Zubek, G. C. King, P. M. Rutter, and F. H. Read, J. Phys. B **22**, 3411 (1989).

[15] A. Menzel, S. P. Frigo, S. B. Whitfield, C. D. Caldwell, M. O. Krause, J-Z. Tang, and I. Shimamura, Phys. Rev. Lett. **75**, 1479 (1995); A. Menzel, S. P. Frigo, S. B. Whitfield, C. D. Caldwell, and M. O. Krause, Phys. Rev. A **54**, 2080 (1996).

[16] J. M. Rost and J. S. Briggs, J. Phys. B **23**, L339 (1990).

[17] H. R. Sadeghpour and C. H. Greene, Phys. Rev. Lett. **65**, 313 (1990).

[18] G. Tanner, K. Richter, and J. M. Rost, Rev. Mod. Phys. **72**, 497 (2000).

[19] C.-N. Liu and A. F. Starace, Phys. Rev. A **59**, R1731 (1999); Phys. Essays **13**, 215 (2000).

[20] U. Fano and C. M. Lee, Phys. Rev. Lett. **31**, 1573 (1973).

[21] P. F. O'Mahony and C. H. Greene, Phys. Rev. A **31**, 250 (1985); C. H. Greene and L. Kim, *ibid.* **38**, 5953 (1988); C. H. Greene, in *Fundamental Processes of Atomic Dynamics*, edited by J. S. Briggs, H. Kleinpoppen, and H. O. Lutz (Plenum, New York, 1988), pp. 105–127.

[22] C. Pan, A. F. Starace, and C. H. Greene, Phys. Rev. A **53**, 840 (1996).

[23] M. Aymar, C. H. Greene, and E. Luc-Koenig, Rev. Mod. Phys. **68**, 1015 (1996).

[24] See, for example, C. N. Liu and A. F. Starace, Phys. Rev. A **60**, 4647 (1999).

[25] H. Le Rouzo and G. Raseev, Phys. Rev. A **29**, 1214 (1984).

[26] K. Smith, *The Calculation of Atomic Collision Processes* (Wiley, New York, 1971).

[27] A. Burgess, Proc. Phys. Soc. London **81**, 442 (1963).

[28] A. F. Starace, in *Handbuch der Physik, Vol. 31: Corpuscles and Radiation in Matter*, edited by W. Mehlhorn (Springer, Berlin, 1982).

[29] R. Püttner, M. Domke, B. Gremaud, M. Martins, A. S. Schlachter, and G. Kaindl, J. Electron Spectrosc. Relat. Phenom. **101-103**, 27 (1999).

[30] Y. Yan and M. J. Seaton, J. Phys. B **20**, 6409 (1987); J. A. Fernley, K. T. Taylor, and M. J. Seaton, *ibid.* **20**, 6457 (1987).

[31] D. E. Herrick, Adv. Chem. Phys. **52**, 1 (1983); D. R. Herrick and A. O. Sinanoglu, Phys. Rev. A **11**, 97 (1975); D. R. Herrick and M. E. Kellman, *ibid.* **21**, 418 (1980); D. R. Herrick, M. E. Kellman, and R. D. Poliak, *ibid.* **22**, 1517 (1980); M. E. Kellman and D. R. Herrick, *ibid.* **22**, 1536 (1980).

[32] C. D. Lin, Phys. Rev. Lett. **51**, 1348 (1983); Adv. At. Mol. Phys. **22**, 77 (1986).

[33] J. M. Feagin and J. S. Briggs, Phys. Rev. Lett. **57**, 984 (1986); Phys. Rev. A **37**, 4599 (1988).

[34] J. M. Rost, J. S. Briggs, and J. M. Feagin, Phys. Rev. Lett. **66**, 1642 (1991); J. M. Rost, R. Gersbacher, K. Richter, J. S. Briggs, and D. Wintgen, J. Phys. B **24**, 2455 (1991).

[35] A. Vollweiter, J. M. Rost, and J. S. Briggs, J. Phys. B **24**, L155 (1991).

[36] J. E. HunterIII and R. S. Berry, Phys. Rev. A **36**, 3042 (1987).

[37] J. M. Rost and J. S. Briggs, J. Phys. B **24**, 4293 (1991).

[38] D. Wintgen and H. Friedrich, Phys. Rev. A **35**, 1628 (1987).